Supporting Information

Behavior of antimony(V) during the transformation of ferrihydrite and its environmental implications

Satoshi Mitsunobu, Chihiro Muramatsu, Katsuaki Watanabe, and Masahiro Sakata

Supplemental texts for Materials and Methods section

Preparation of model compounds for Sb XAFS analysis.

Sb(V)-coprecipitated ferrihydrite, goethite, and hematite

Sb(V)-coprecipitated ferrihydrite for EXASF reference was prepared using the same preparation method described in main body of present paper. Sb(V)-coprecipitated goethite was synthesized from mixed $FeCl_3$/Sb(V) solutions following the procedure given by Schwertmann and Cornell (2000) describing preparation of Al-substituted goethite. 100 mL of solutions containing different Sb/Fe molar ratios (mixture of 0.25 M $FeCl_3$ and 10 mM $NaSb(OH)_6$ solutions) were mixed with 250 ml of 1.0 M KOH to ensure alkaline conditions around pH12 to induce the Sb(V)-coprecipitated ferrihydrite. The solutions were placed in an oven at 70°C for 2 weeks. After crystallization was completed, solid samples were washed twice with 1.0 M KOH and distilled water, and then dried.

Sb(V)-coprecipitated hematite was synthesized from mixed $Fe(NO_3)_3$/Sb(V) solutions following the procedure given by Schwertmann and Cornell (2000) describing preparation of Al-substituted hematite. 100 mL of solutions containing different Sb/Fe molar ratios (mixture of 0.25 M $FeCl_3$ and 10 mM $NaSb(OH)_6$ solutions) were mixed with 120-150 ml of 1.0 M KOH to bring the pH to 7.0. After complete precipitation, the precipitates were washed with distilled water, made up to 100 ml total volume with distilled water, and adjusted again to pH 7.0 with HNO_3. The suspensions were stored for 20 days at 80 °C with occasional shaking, after which the samples were washed four times with Milli-Q water.

For both Sb(V)-coprecipitated goethite and hematite, poorly crystalline materials (e.g., ferrihydrite and any salts) and adsorbed species contaminated in the solids were purified before analysis by treating the solids with 100 mL 1.0 M H_2SO_4 for 5 h at 50 °C in a waterbath. Mineralogical purity was checked by XRD analysis (Figure S1 in SI). The suspensions was filtered through a 0.2 μm cellulose membrane filter and stored until needed. The Sb/Fe molar ratios in Sb(V)-coprecipitated solids were determined by dissolving the solid completely in 6.0 M HCl at 50 °C.

An Sb/Fe molar ratio of 0.005 is selected for Sb EXAFS analysis of each model compound, because Sb loading level did not influence on the EXAFS spectral features at least in range of Sb/Fe = 0.001-0.01.

Sb(V)-sorbed goethite, hematite, and ferrihydrite

Goethite, hematite, and two-line ferrihydrite for sorption samples were synthesized following the method of reference (Schwertman and Cornell, 2000). For the preparation of ferrihydrite (two-line), we prepared 30 mL of a 0.06 M Fe(III) solution by dissolving $FeCl_3 \cdot 6H_2O$ in Milli-Q water. The pH of the solution was brought to ~7.5 in about 5 min using 1.0 M NaOH solution, and was maintained at that pH for 24 h with the slurry mechanically agitated. Goethite was prepared by hydrolysis of ferric chloride in an alkaline system at 70 °C. Hematite was

synthesized by transformation of two-line ferrihydrite at 90 °C and pH 8-8.5 for 14 days. These products were also used as reference materials for the least-squares fitting of Fe EXAFS.

The phase identity of synthesized goethite, hematite, and ferrihydrite was confirmed by powder XRD of the dried samples, and the patterns were consistent with published data of these minerals (Figure S1 in SI). The synthesized goethite, hematite, and ferrihydrite were washed by Milli-Q water at least five times to remove chloride ions, and the slurries were finally prepared by adding appropriate amount of Milli-Q water. The Fe content in these slurries used in the experiment was determined by measuring the Fe abundance in dissolved slurries in 6 M HCl by ICP-OES (Varian 730-ES).

Sb(V) sorption on the ferrihydrite, goethite, and hematite was conducted at various initial Sb(V) concentrations and a constant ionic strength (I = 0.01 M, $NaNO_3$). Five mL of the ferrihydrite suspension which contained 2.10×10^{-4} mol of Fe(III) and a supporting electrolyte solution were placed in a 50 mL glass tube. For the goethite and hematite series, 5 mL of the Fe(III) oxide suspension was also set in place of ferrihydrite. Then, an appropriate amount of 9.5 mM potassium antimonate ($KSb(OH)_6$) solution was added to produce the desired Sb/Fe molar ratio in the slurries of goethite, ferrihydrite, and hematite. The total volume of the solution was 30 mL and the pH of the solution was adjusted to 6.0 ± 0.05 by addition of 0.1 or 0.01 M NaOH solution. At this pH, Sb(V) predominantly occurs in the form of $Sb(OH)_6^-$ (Filella et al., 2003). The suspension with the Sb(V)-containing solution was placed in a wave-motion shaker at 25 ± 0.5 °C for 24 h. Afterwards, the pH of the suspension was measured and each solution was filtered through a 0.2 μm cellulose membrane filter.

TEM analyses of the solid samples.

Transmission electron microscopy (TEM) analysis was performed using a JEM-2010 (JEOL) with an accelerating voltage of 200 kV. The TEM analysis was conducted in the most aged samples (70 days) with Sb/Fe ratios of 0.001 and 0.01. Small amounts of the solid samples were collected by a clean spatula and dispersed in methanol in an ultrasonic bath (Utsunomiya et al., 2009). A drop of the resulting suspension was placed on a perforated carbon mesh supported by a Cu-grid.

FT-IR analyses of the solid samples.

Fourier transform infrared (FT-IR) spectra were recorded at RT using a FT/IR-4200 (JASCO). The FT-IR spectrometer was connected to a PC with the installed IR data manager program to process the recorded spectra. The IR spectra were measured in air after evacuation of samples at 100 °C for 2h according to Kandori et al. (1998). The specimens were pressed into small discs using a spectroscopically pure KBr matrix (1 mg solid in 500 mg KBr).

Table S1. Amount of each mineral in aged solids estimated by linear combination fitting of Fe EXAFS.

Control (without Sb)

Aging time (d)	goethite (%)	error (%)	hematite (%)	error (%)	ferrihydrite (%)	error (%)	R factor (%)
0	0	0	0	0	100	0	-
14	21.7	1.9	12.2	1.0	66.1	2.2	2.9
26	31.8	1.7	21.7	0.9	46.6	1.9	2.0
42	53.6	1.9	28.5	1.0	22.0	2.1	1.8
56	47.4	1.8	29.1	0.9	23.5	2.0	1.7
70	54.0	1.9	31.8	1.0	14.2	2.1	1.6

Sb/Fe = 0.001

Aging time (d)	goethite (%)	error (%)	hematite (%)	error (%)	ferrihydrite (%)	error (%)	R factor (%)
0	0	0	0	0	100	0	-
14	26.3	1.6	17.7	0.8	56.0	1.8	2.0
26	40.7	1.9	24.9	1.0	34.4	2.1	2.2
42	50.3	1.9	28.4	1.0	21.3	2.2	2.0
56	54.1	2.4	32.0	1.2	14.0	2.7	2.5
70	51.9	2.0	35.2	1.0	13.0	2.2	1.8

Sb/Fe = 0.005

Aging time (d)	goethite (%)	error (%)	hematite (%)	error (%)	ferrihydrite (%)	error (%)	R factor (%)
0	0	0	0	0	100	0	-
14	33.7	1.4	11.3	0.7	55.1	1.6	1.3
26	50.0	1.7	16.2	0.9	33.8	1.9	1.7
42	55.4	1.9	19.8	1.0	24.8	2.1	2.0
56	65.2	1.8	19.7	0.9	15.2	2.0	1.6
70	68.9	2.1	19.7	1.0	11.4	2.3	2.1

Sb/Fe = 0.01

Aging time (d)	goethite (%)	error (%)	hematite (%)	error (%)	ferrihydrite (%)	error (%)	R factor (%)
0	0	0	0	0	100	0	-
14	37.5	1.6	9.1	0.8	53.4	1.8	1.6
26	55.7	2.1	10.4	1.0	34.0	2.3	2.4
42	65.6	2.2	13.0	1.1	21.4	2.5	2.4
56	70.0	2.4	14.6	1.1	15.4	2.6	2.5
70	72.0	2.3	13.9	1.1	14.1	2.6	2.4

Table S2. Structual data on the local environment of Sb derived from the simulation of EXAFS data of aged solids (Sb/Fe ratio = 0.001 and 01) and model compounds (Sb(V)-coprecipitated ferrihydrite, goethite, and hematite with Sb/Fe ratio of 0.005).
CN = coordination number, R = interatomic distance, ΔE_0 = threshold E_0 shift and σ^2 = Debye-Waller factor.
Fits were performed over the k range: 2.0-13.0 Å^{-1}. The estimated standard deviations in least-squares fit are given in parenthese and refer to the estimated error in the last decimal place.

	Sb-O				First Sb-Fe shell (Sb-Fe$_1$; Face / Edge)				Second Sb-Fe shell (Sb-Fe$_2$; Corner)				Third Sb-Fe shell (Sb-Fe$_3$; Corner')			
sample	**R (Å)**	**CN**	**ΔE_0 (eV)**	**σ^2**	**R (Å)**	**CN**	**ΔE_0 (eV)**	**σ^2**	**R (Å)**	**CN**	**ΔE_0 (eV)**	**σ^2**	**R (Å)**	**CN**	**ΔE_0 (eV)**	**σ^2**
Sb/Fe = 0.001																
0 d	1.98 (1)	6.0 (5)	3.47	0.005	3.08 (2)	1.4 (5)	-	0.006	3.54 (3)	2.0 (5)	-	-				
14 d	1.96 (1)	6.0 (5)	2.45	0.005	3.08 (2)	2.3 (5)	-	0.006	3.53 (3)	2.7 (6)	-	-				
42 d	1.97 (1)	6.0 (5)	2.50	0.004	3.07 (2)	2.6 (5)	-	0.006	3.53 (3)	3.1 (6)	-	-				
70 d	1.97 (1)	6.0 (5)	2.74	0.005	3.07 (2)	3.2 (6)	-	0.006	3.52 (2)	2.6 (6)	-	-				
Sb/Fe = 0.01																
0 d	1.97 (1)	6.0 (5)	2.76	0.005	3.09 (2)	1.6 (4)	-	0.006	3.54 (1)	2.1 (4)	-	-				
14 d	1.97 (1)	6.0 (5)	2.65	0.005	3.08 (2)	2.1 (6)	-	0.006	3.54 (2)	2.2 (6)	-	-				
42 d	1.97 (1)	6.0 (4)	2.59	0.005	3.08 (2)	2.4 (6)	-	0.006	3.55 (2)	3.6 (6)	-	-				
70 d	1.97 (1)	6.0 (5)	2.32	0.005	3.08 (2)	2.4 (6)	-	0.006	3.56 (2)	3.6 (6)	-	-				
Sb(V)-coprecipitated ferrihydrite	1.97 (1)	6.0 (4)	2.97	0.004	3.08 (2)	1.3 (6)	-	0.005	3.56 (2)	2.0 (6)	-	-				
Sb(V)-coprecipitated goethite	1.97 (1)	6.3 (5)	3.40	0.005	3.11 (2)	2.0 (6)	-	0.005	3.57 (2)	6.0 (5)	-	-				
Sb(V)-coprecipitated hematite	1.97 (1)	6.0 (5)	2.82	0.005	3.05 (1)	4.1 (6)	-	0.007	3.48 (2)	3.0 (6)	-	-	3.70 (1)	4.9 (6)	-	-

Fittings were performed by fixing a ΔE for all shells and a Debye-Waller factor for Sb-Fe shells.
The uncertainty in the analysis was evaluated by R factor given by next equation.

$$R = \Sigma\{k^n\chi_{obs}(k) - k^n\chi_{cal}(k)\}^2 / \Sigma\{k^n\chi_{obs}(k)\}^2$$

XRD analysis of model compounds

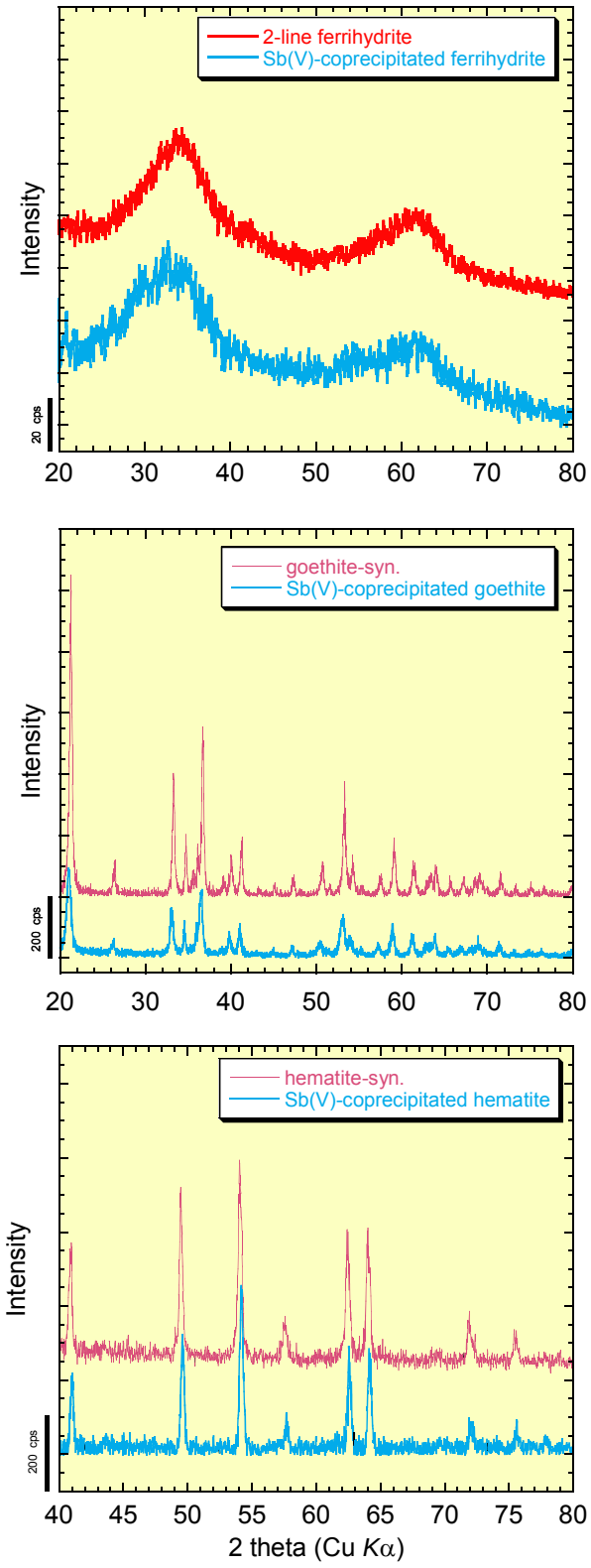

Figure S1. XRD patterns of Sb(V)-coprecipitated ferrihydrite, goethite, hematite (blue line), and its Sb free synthesized mineral phases (red line). Sb/Fe molar ratio in coprecipitated samples is 0.005.

XRD and Fe EXAFS analyses of aging samples

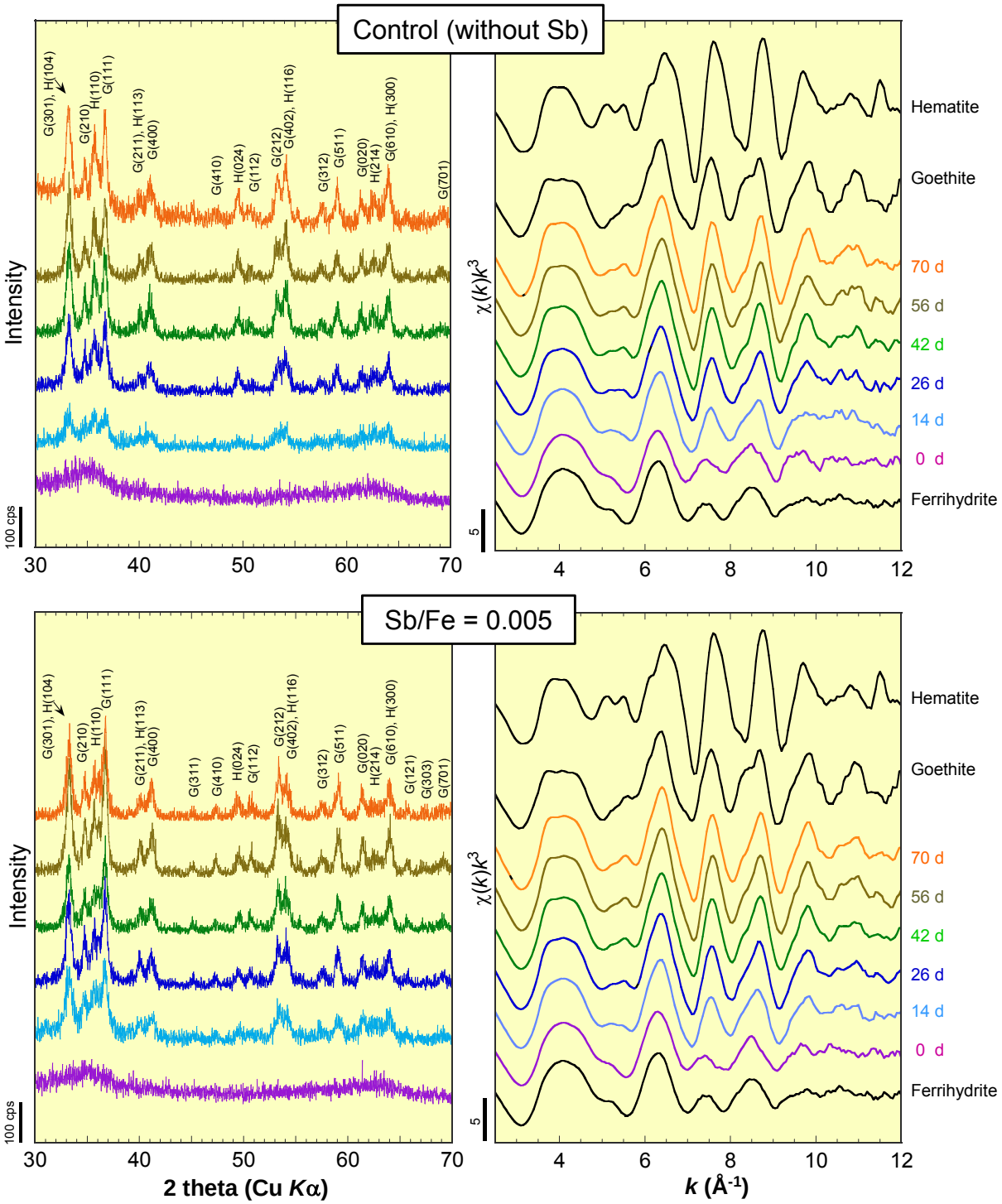

Figure S2. Time series XRD (left) and Fe EXAFS (right) of aged solid samples at control and Sb/Fe = 0.001-0.01. In figures, "H" and "G" stand for hematite and goethite, respectively.

Fe XANES analyses of aging samples

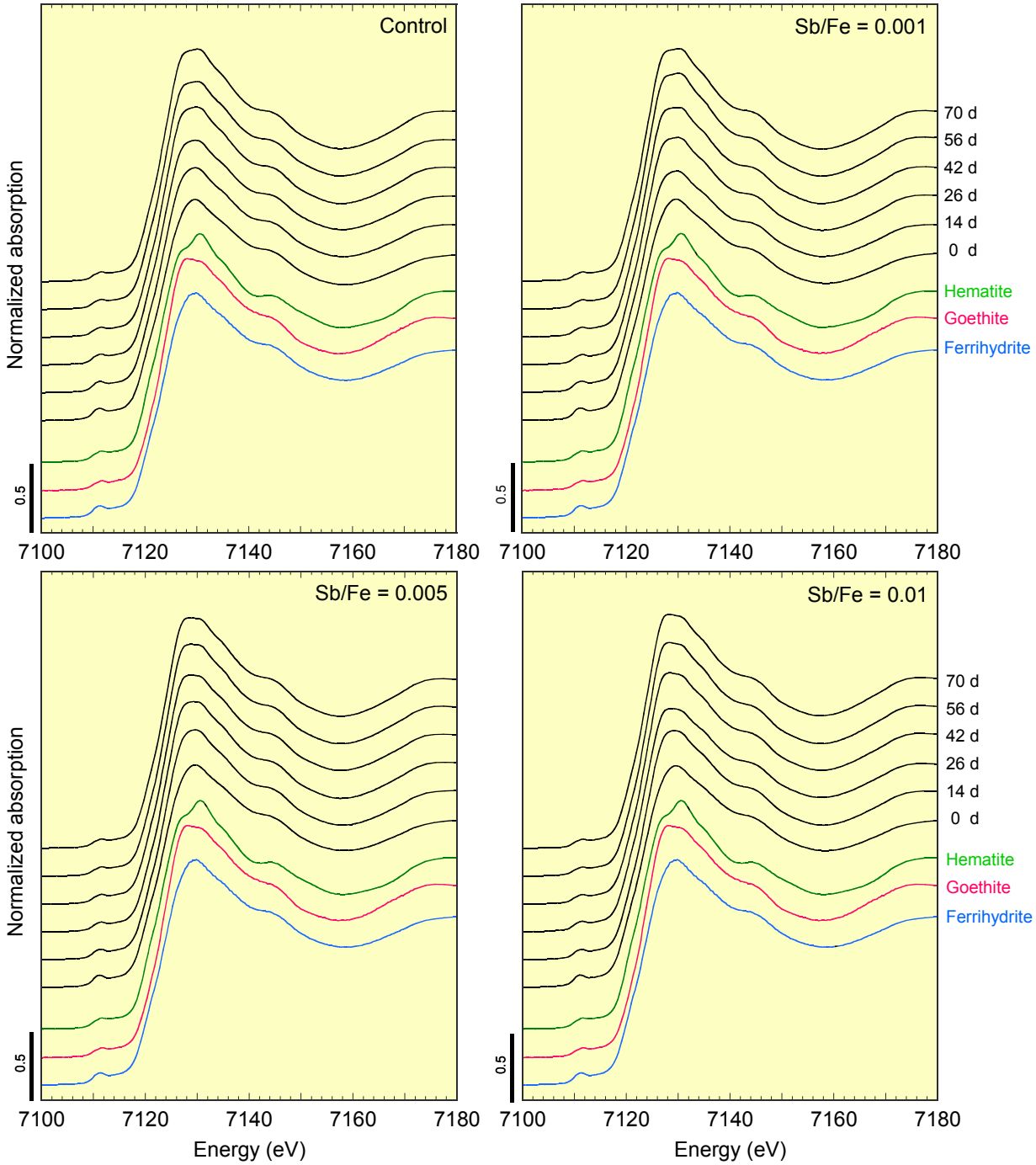

Figure S3. Time series Fe K-edge XANES spectra at Sb/Fe molar ratio = 0 (control), 0.001, 0.005, and 0.01.

Linear combination fit of Fe EXAFS

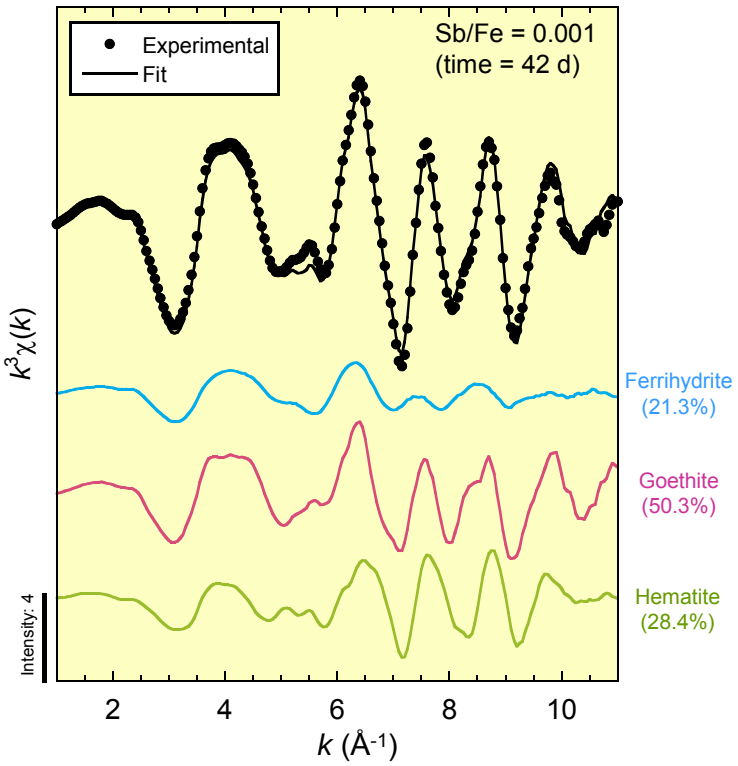

Figure S4. A example of least-squares fitting using Fe EXAFS spectra. The fitting range is k = 1.0-11.0 Å^{-1}.

Time series Fourier transform spectra of Fe EXAFS

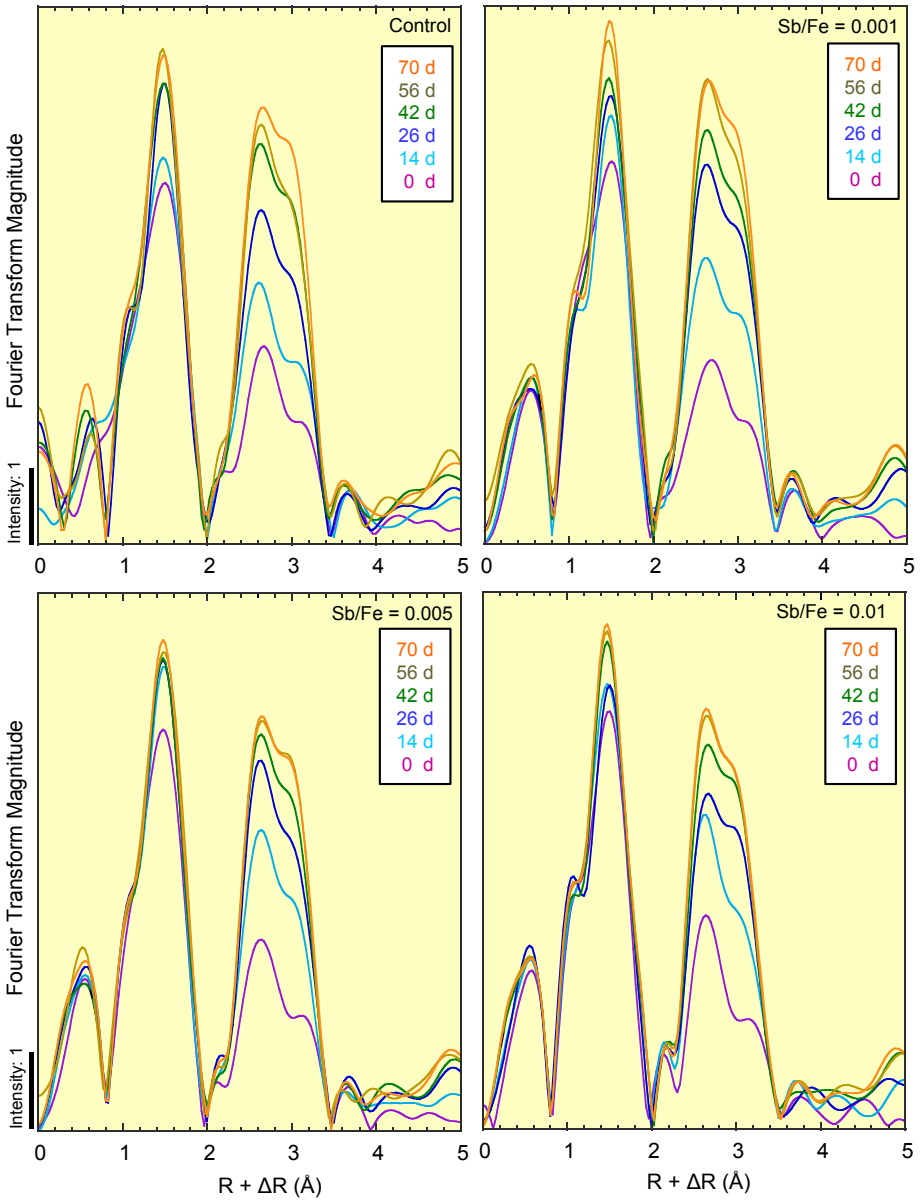

Figure S5. Time series Fourier transform spectra of k^3-weighted Fe EXAFS at control (a) and Sb/Fe molar ratios = 0.001 (b), 0.005 (c), and 0.01 (d). FT from k to r space was performed in a range of 2.5-12.0 Å for all samples.

Preferential goethite formation in the presence of Sb(V)

Goethite/hematite ratios in aged products in Figure S7 were shown as a function of aging time for all systems, and were larger at higher Sb/Fe ratio throughout entire period of aging. These results clearly suggest that goethite were preferentially formed in the transformation of ferrihydrite in the presence of Sb(V), which is consistent with results of XRD analysis.

Cornell and Schwertmann (2003) indicated that this preferential goethite formation would be induced by either acceleration of goethite formation or retardation of hematite formation. When the acceleration of goethite formation occurs at Sb loading, it follows that the overall transformation of ferrihydrite is also accelerated. However, transformation rate of ferrihydrite did not change with Sb loading in present study (Table S1). Thus, these findings indicate that the preferential goethite formation observed is due to retardation of hematite formation at high Sb loading, because the goethite and hematite are formed from ferrihydrite by competing mechanisms (Cornell and Schwertmann, 2003). Conditions that promote goethite are unfavorable for hematite formation. The hematite formation from the ferrihydrite involves a combination of aggregation of ferrihydrite, dehydration, and rearrangement processes (Fisher and Schwertmann, 1975). Cornell and Schwertmann (2003) suggested that formation of the hematite is often retarded in the presence of foreign compound when the aggregation of ferrihydrite, first step in the hematite formation, is blocked. They also suggested that the aggregation of ferrihydrite is suppressed by increase of electrostatic repulsion between ferrihydrite particles. In this study, the Sb(V)-doped ferrihydrite used were synthesized by coprecipitation with Sb(V) (not by sorption). Mitsunobu et al. (2010) reported that most of Sb(V) in Sb(V)-coprecipitated ferrihydrite are incorporated into the structure by substituting Fe(III) sites, based on the spectroscopic evidence. They also indicate that large difference in charge between the guest cation (Sb^{5+}) and the host cation (Fe^{3+}) may affect entire charge balance of the solid even at low Sb loading. Thus, we speculate as a hypothesis that the Sb(V) incorporated into ferrihydrite interferes the aggregation of the particles and retards the hematite formation, which leads to the preferential goethite formation observed. In fact, it has been reported that incorporation of Ti(IV) (higher valent number than Fe(III)) into ferrihydrite enhances the formation of goethite over hematite (Fitzpatrick et al., 1978) at similar metal/Fe ratio and pH to present study, which may support our hypothesis. However, in order to demonstrate the hypothesis, further investigation on surface charge of the Sb(V)-coprecipitated ferrihydrite is needed. As another possible scenario to explain the preferential goethite formation, a difference in crystal structure of goethite and hematite could be mentioned. When Sb(V) is incorporated into crystal structure, the goethite can balance the charge difference by releasing protons from the structure, while the hematite has not protons in the structure to release and is therefore retarded.

Goethite/Hematite ratio in aged solids

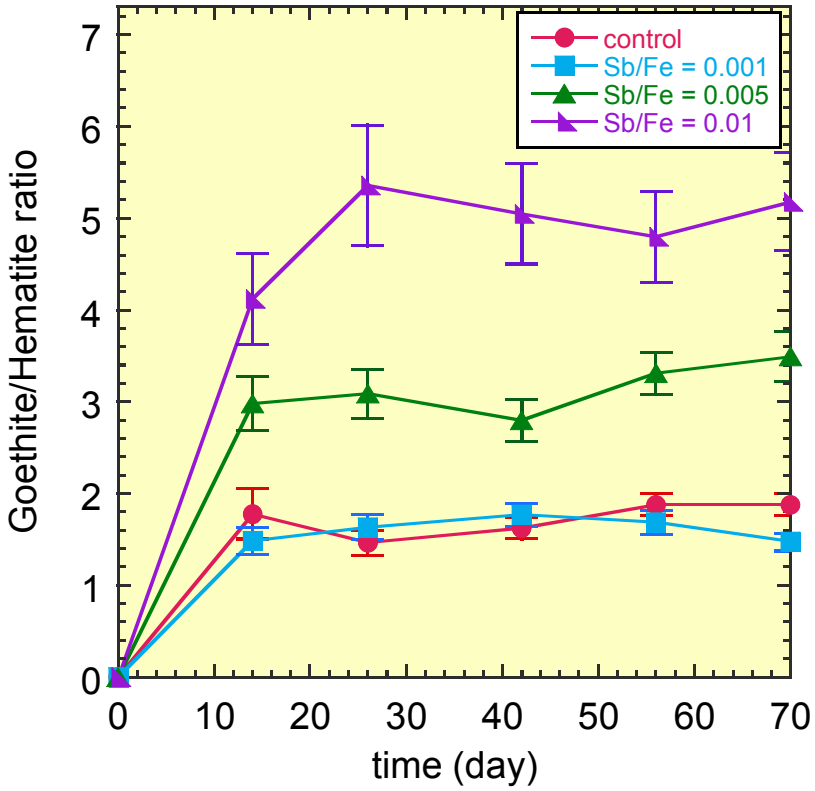

Figure S6. Goethite/Hematite ratio in aged solids at Sb/Fe = 0 (control), 0.001, 0.005, and 0.01.

Sb XANES analyses of aged samples

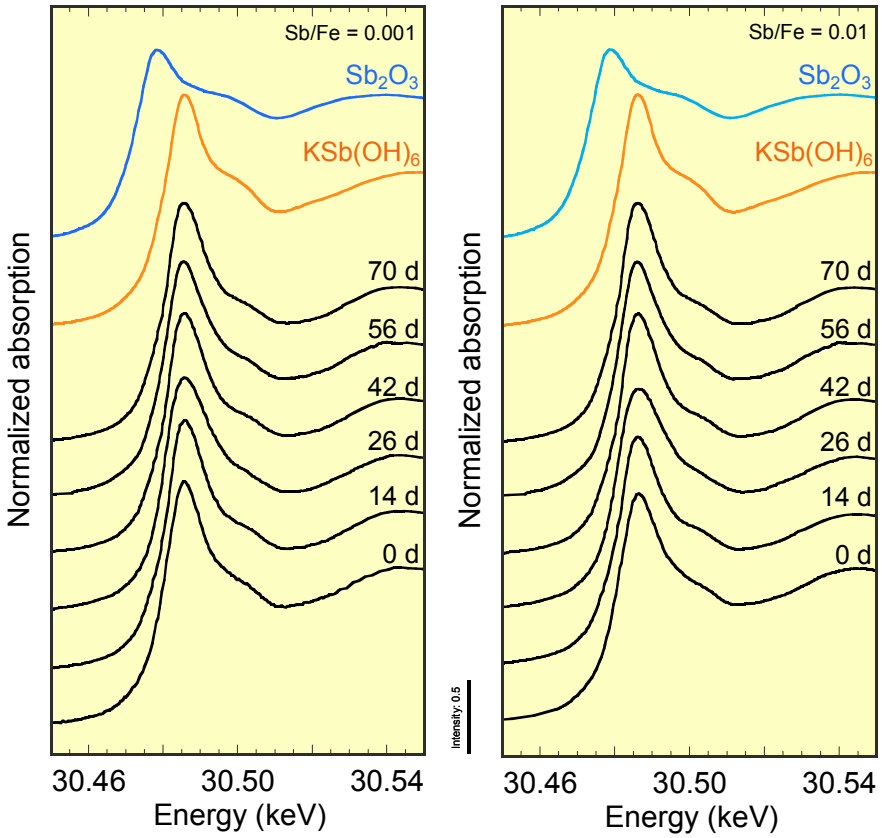

Figure S7. Sb K-edge XANES spectra of aged samples (Sb/Fe molar ratio = 0.001 and 0.01) and reference samples ($Sb^{III}_2O_3$ and $KSb^{V}(OH)_6$). Sb XANES analyses of solid samples showed that oxidation states of Sb in the solids were consistently pentavalent Sb(V) and did not change with aging.

Sb EXAFS analysis of coprecipitated model compounds

Sb(V)-coprecipitated ferrihydrite

The Sb EXAFS and the FT of Sb(V)-coprecipitated ferrihydrite, goethite, and hematite are shown in Figures 3 and 4c. On the Sb(V)-coprecipitated ferrihydrite, in the FT, three main peaks were shown in R+ΔR = 1.0-3.5 Å (phase-shift uncorrected, Figure 4c). The first peak at R+ΔR = 1.5 Å corresponds to the O coordination shell and the two other peaks at R+ΔR = 2.5-3.4 Å corresponds to Fe coordination according to previous study (Mitsunobu et al., 2010). The quantitative analysis of the first coordination (Sb-O) shell showed that all six O atoms were at the same distance (1.97 Å) from the central Sb (Table S2). This octahedral Sb-O linkage is characteristic for a pentavalent Sb (Scheinost et al., 2006). The two peaks of Sb-Fe shells in the FT at 2.6 Å and 3.1 Å in Figure 6 (phase shift uncorrected) were simulated by a two-shell fitting model. The two fitted Sb-Fe distances were 3.08 Å and 3.56 Å, respectively (Table S2). The first value corresponds to the Sb-Fe distance along the edge-sharing linkage and the second corresponds to the Sb-Fe distance along the corner-sharing link. The CNs of both bonds were 1.3 and 2.0, respectively, and the total value was 3.3 (1.3 + 2.0). This CN value is significantly larger than that in the case of the inner-sphere adsorption complex for Sb(V) on Fe(III) oxyhydroxides (< 2, Leuz et al., 2006). Thus, the larger CNs of the Sb-Fe shells in the Sb(V)-coprecipitated ferrihydrite indicate that Sb(V) is incorporated into the ferrihydrite structure. These findings are also consistent with the published data of the Sb(V) coprecipitated with ferrihydrite (Mitsunobu et al., 2010). In addition, the CNs of Sb-Fe shells in Sb(V)-coprecipitated ferrihydrite were relatively smaller than those of the Fe-Fe shells in pure ferrihydrite. This may be due to (i) the increase of disorder of Fe-Fe links in ferrihydrite structure by Sb(V) incorporation and/or (ii) the mixing of adsorbed species present in Sb(V)-coprecipitated ferrihydrite (less than 10%, Table S1). Similar reduction of CN for the metal-Fe shell in substituted ferrihydrite was observed with Cr(III) substitution into ferrihydrite (Hansel et al., 2003). Moreover, Figure S9a shows the Fourier filtered Sb-O and Sb-Fe contributions to the EXAFS of Sb(V)-coprecipitated ferrihydrite. The position of a specific peak around k = 7 Å^{-1} clearly overlapped with the maximum of the Sb-Fe wave. Thus, this indicates that the specific peak observed was due to the contribution of the Sb-Fe shell in the structure.

Sb(V)-coprecipitated goethite

XRD pattern of Sb(V)-coprecipitated goethite are shown in Figure S11a. All peaks in their patterns could be assigned to those of goethite. Using the peak positions, unit cell length for edge *a* in goethite structure was calculated (Figure S11b). As a result, the cell length increased with higher Sb/Fe ratio, indicating an expansion of goethite unit cell. In addition, a linear relationship was observed between unit cell length and Sb/Fe ratio in solid, and its line slope was

positive (Figure S12b). Considering the ionic radius of Sb(V) (= 0.060 nm, Shanon et al., *Acta Cryst.*, 1986), the slope value (= 0.32) was also comparable to those of other cations (Figure S12c; Gerth, *Geochim. Cosmochim. Acta*, 1990). Considering previous reports for other ions, these findings indicate that Sb(V) is structurally incorporated into goethite (Stiers and Schwertmann, *Geochim. Cosmochim Acta*, 1985; Ebinger and Schulze, *Clays Clay Min.*, 1989; Schwertmann et al., *Geochim. Cosmochim Acta*, 1989). Furthermore, FT-IR analysis showed that in the Sb(V)-coprecipitated goethite, the peak at 890 cm^{-1} shifted to low wavenumber with higher Sb content (Figure S12d). Previous studies documented that the peak at 890 cm-1 corresponds to OH bending band at the (001) plane and its peak shift is often caused by cation substitution into goethite (Gasser et al., *Clay Min.*, 1996; Cornell and Schwertmann, *The Iron Oxides*, 2003). Thus, the IR spectroscopy also suggested that Sb(V) is structurally incorporated into goethite. To investigate the coordination environment of Sb(V) in goethite structure in detail, Sb EXAFS analysis of Sb(V)-coprecipitated goethite was conducted. In the Fourier transform (FT) of Sb(V)-coprecipitated goethite, the first strong peak corresponding ($R+\Delta R$ = 0.8-2.0 Å) to the O coordination and the other two peaks corresponding to the contributions from the Sb-Fe shells were observed ($R+\Delta R$ = 2.5-3.5 Å in Figure 6c). Quantitative analysis of the Sb-O peak shows that the Sb-O bond distance was 1.97 Å and its CN was nearly six, showing the substitution of Sb(V) octahedron into the Fe(III) octahedral site in goethite. For the next nearest-neighbor shell (Sb-Fe shell), a two-shell model was used to fit, because goethite has two edge-sharing links of Fe-Fe (E and E') and one double corner-sharing link of Fe-Fe (DC) in the structure (Figure S8) and the bond distances of E' and DC are relatively close (Manceau and Drits, *Clay Min.*, 1993; Hansel et al., *Geochim. Cosmochim. Acta*, 2003). The analysis showed two Sb-Fe distances of 3.11 Å and 3.57 Å (Table S2). The first value corresponds to the edge-sharing link between two adjacent octahedra (Mitsunobu et al., *Environ. Sci. Technol.*, 2010). The second distance corresponds to Sb-Fe distance in mixture of both another edge-sharing and the double-corner sharing linkages (Figure S8). The CNs of two Sb-Fe shells were 2.0 and 6.0, respectively. These findings indicate that Sb(V) in goethite has a similar coordination environment to that of Fe(III) in goethite, and that Sb(V) is distributed uniformly over the goethite structure, which is consistent with the XRD and FT-IR results. On the other hand, we need further evidence to strongly suggest the "isomorphous substitution of Sb(V) in goethite", such as occurrence of coupled substitution, as Reviewer 1 indicated. However, our approaches alone will not be enough to examine the coupled substitution (Singh et al., *Clays Clay Min.*, 2000), and it is also out of main scope of this paper. Thus, we do not suggest "isomorphous substitution" in this paper but "structural incorporation" or "heterovalent substitution". Related parts in the manuscript were corrected for the revision.

Moreover, Figure S9 shows the contribution of Sb-O and Sb-Fe shells to the experimental spectrum of Sb(V)-coprecipitated goethite. The positions of specific peaks around k = 7 and 9 $Å^{-1}$ overlap with the maximum of the Sb-Fe contribution. This indicates that the specific peaks

observed in EXAFS of Sb(V)-coprecipitated goethite were derived from the contribution of Sb-Fe shells with higher CN, similar to the case of Sb(V)-ferrihydrite.

Sb(V)-coprecipitated hematite

In the Sb(V)-coprecipitated hematites, the shift of several peaks was also observed in their XRD patterns (Figure S13a). In addition, broadening of peaks was found in higher Sb(V) loading, which implies a formation of defect in the structure. Calculated unit cell length for edge *a* increased from 0.5037 to 0.5050 nm within Sb/Fe ratio of 0.001-0.01 (Figure S13b), indicating an expansion of hematite unit cell. Moreover, a linear relationship between the *a* edge length and Sb content was observed (Figure S13b). Previous studies have reported for other cations (e.g., Al, Cu, Ni, Nd) that the edge length systematically varies with cation contents when they are substituted into the structure (Cornell and Giovanoli, *Polyhedron*, 1988; Cornell et al., *J. Chem. Tech. Biotechnol.*, 1992; Nagano et al., *Clays Clay Min.*, 1999). Thus, these findings and reports indicate that Sb(V) is incorporated in the hematite structure. We also performed FT-IR analysis of the Sb(V)-coprecipitated hematite. Particularly, previous studies suggested that the IR bands around 3400 cm^{-1} of hematite correspond to OH stretch vibrations, and that intensities of the peaks are sensitive to the amount of structural OH^- in hematite lattice (Cornell and Schwertmann, *The Iron Oxides*, 2003). Kandori et al. (*J. Mat. Chem.*, 1998) reported that intensities of the bands increased by the structural OH^- incorporation with metal incorporation into the hematite. In the IR spectra of Sb(V)-coprecipitated hematite, the two bands in 3400 cm^{-1} were observed and the intensities increased in higher Sb/Fe ratio (Figure S13c). Therefore, the increase in the band intensities should be derived from lattice OH^- associated with structural incorporation of Sb(V) in the structure. If this is the case, we can deduce that the incorporation of OH^- was formed by the coupled incorporation to compensate for the charge difference of Sb(V) and Fe(III) ions. Coordination environment of the Sb(V) incorporated into hematite was investigated by Sb EXAFS analysis. In FT of the Sb(V)-coprecipitated hematite, the first strong peak corresponding to the O coordination and the other three peaks corresponding to contributions from the Sb-Fe shells were observed (Figure 6c). Quantitative analysis of the Sb-O peak shows that the Sb-O bond distance was 1.97 Å and its CN was nearly six. For the next nearest-neighbor shells (Sb-Fe shell), a three-shell model was used to fit the Sb-Fe links, because octahedra in hematite share one face (F), three edges (E), three double-corners (DC), and six double corners (DC') as shown in Figure S7 (Manceau and Drits, *Clay Min.*, 1993). The analysis shows three Sb-Fe distances of 3.05 Å, 3.48 Å, and 3.70 Å (Table S2). The first value corresponds to an average distance of the face- and edge-sharing linkages. The second distance corresponds to Sb-Fe distances in the double-corner sharing linkage (DC). The third value corresponds to Sb-Fe linkage of another corner-sharing linkage (DC'). The CN of each Sb-Fe shell was 4.1, 3.0, and 4.9, respectively. These EXAFS findings indicate that Sb(V) is structurally incorporated into hematite with a coordination similar to Fe(III)

in pure hematite, which is agreeable with the XRD and FT-IR analyses of the Sb(V)-coprecipitated hematite.

Moreover, Figure S9 shows the contribution of Sb-O and Sb-Fe shells to the experimental spectrum of Sb(V) coprecipitated with hematite. The positions of specific peaks around k = 7.5 and 9.5 Å^{-1} (dotted lines) overlap with the maximum of the Sb-Fe contributions This indicates that the specific peaks observed in EXAFS of Sb(V)-coprecipitated hematite were derived from the contribution of Sb-Fe bonds, similar to the case of Sb(V)-coprecipitated ferrihydrite and goethite. In fact, the peaks in the k range of 7-9 Å^{-1} were not observed at Sb(V) adsorbed species due to smaller Sb-Fe contribution of the adsorbed Sb(V) (Figure 5). Thus, we can distinguish whether Sb(V) is a incorporated or adsorbed species in ferrihydrite, goethite, and hematite using the EXAFS spectral features in this k space region.

Fe-Fe linkages in structures of hematite and goethite

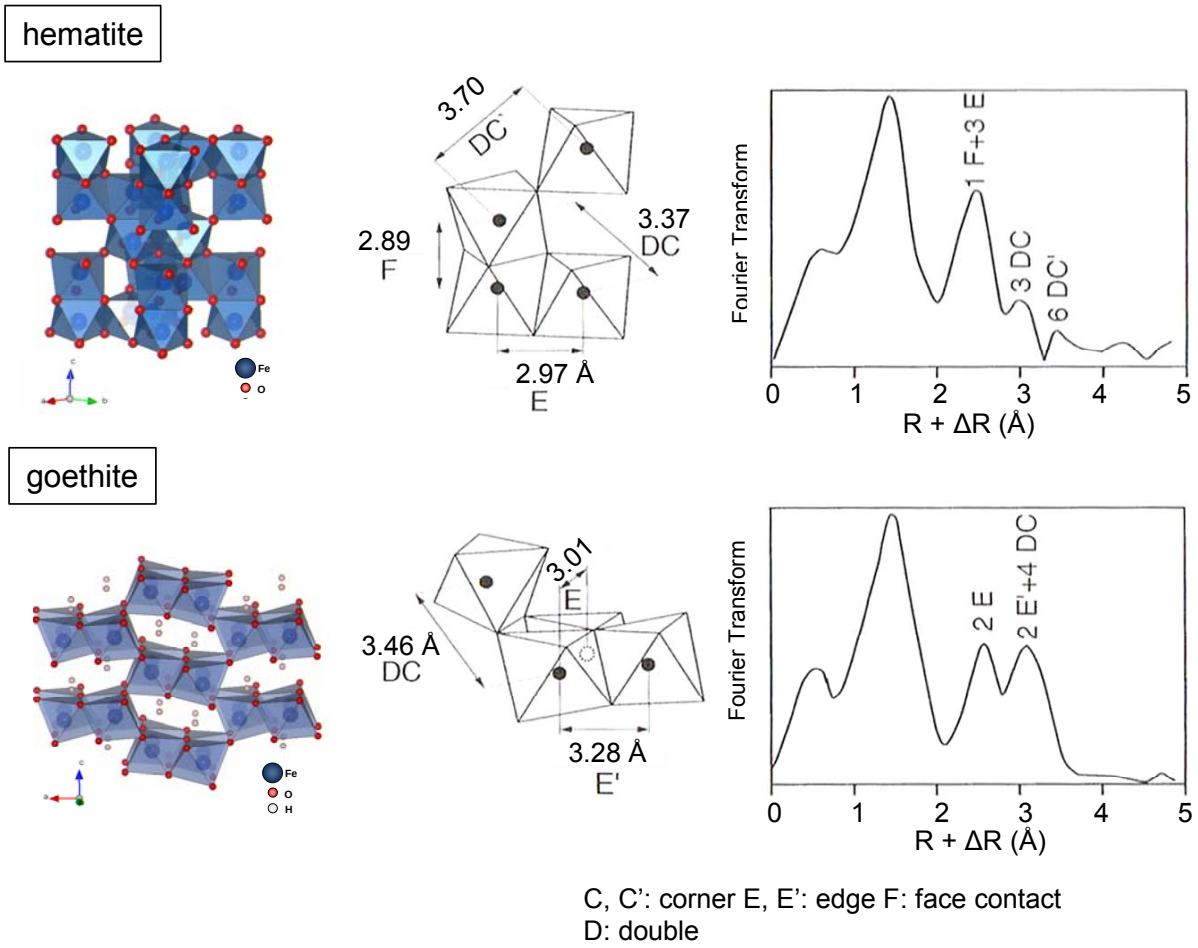

Figure S8. Basic structural units and Fe-Fe distances for hematite and goethite and their associated radial distribution functions as obtained from EXAFS spectra. The first peak in the radial distribution function corresponds to the oxygen shell surrounding the Fe atom and the second and third peaks to nearest and next-to-nearest Fe neighbors (modified from Manceau and Drits (1993)).

Spectra of Fourier filtered Sb-O and Sb-Fe contributions of coprecipitated samples

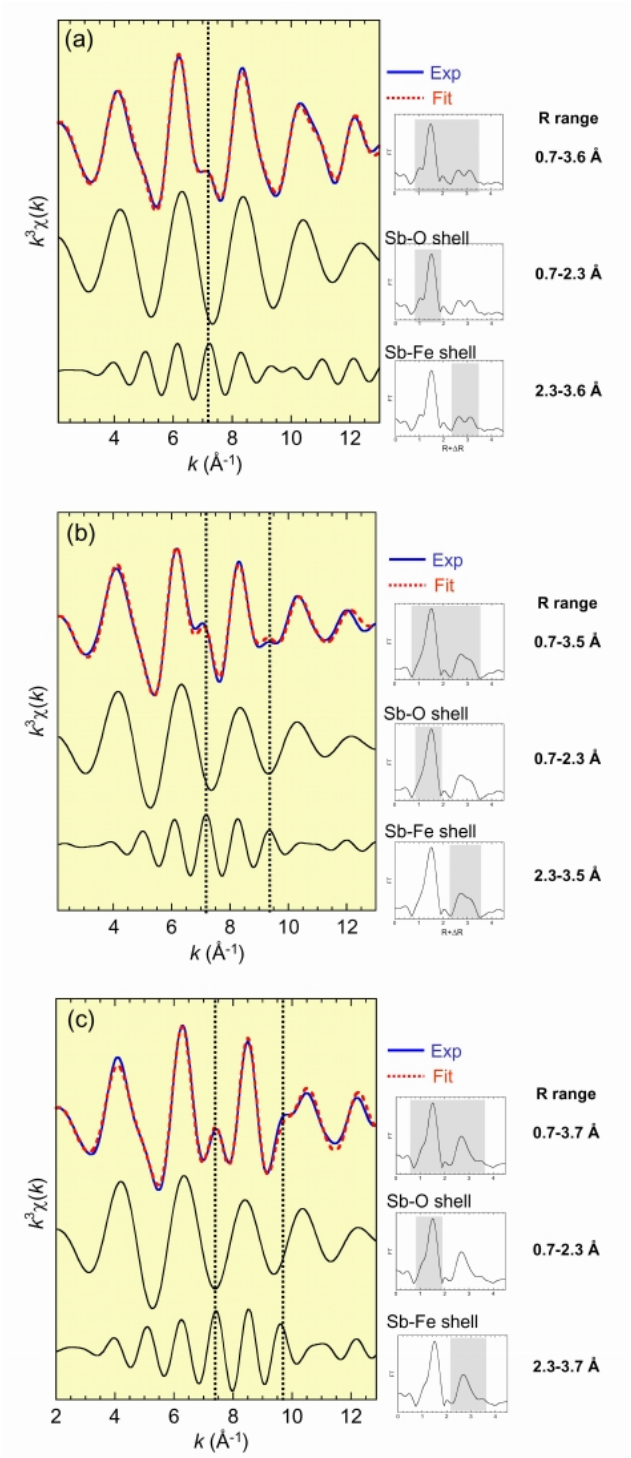

Figure S9. The upper spectra show the sum of Fourier filtered Sb-O and Sb-Fe contributions (blue line) with theoretical spectrum (red dotted line) for simulation of Sb(V)-coprecipitated ferrihydrite (a), goethite (b), and hematite (c). Middle and lower spectra show the Fourier filtered Sb-O and Sb-Fe contributions, respectively. Black dotted bars stand for the wave-number (k) of specific peaks shown in the experimental spectrum around k = 7-10 Å^{-1}. The k positions of the peaks overlap with the maximum of Sb-Fe contribution.

Total coordination numbers (CNs) of Sb-Fe shells in aged samples

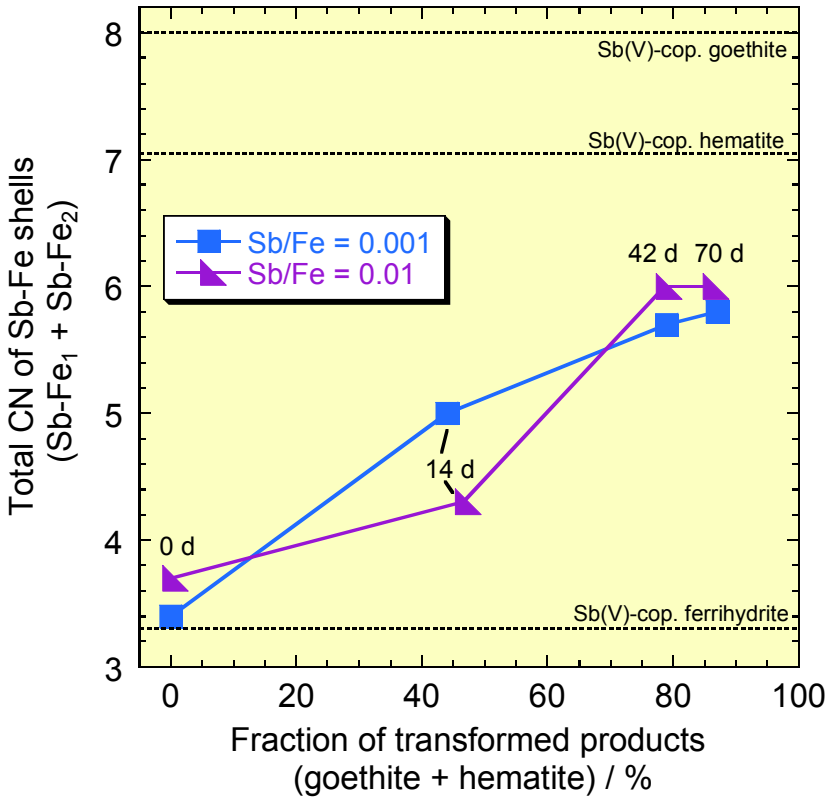

Figure S10. Relationship between CNs of the Sb-Fe bonds and fraction of transformed products in aging samples. The CN values were determined by EXAFS simulations (Table S2). Dotted lines show the CN values of Sb(V)-coprecipitated ferrihydrite, goethite, and hematite determined by EXAFS simulations.

TEM analyses of aged samples

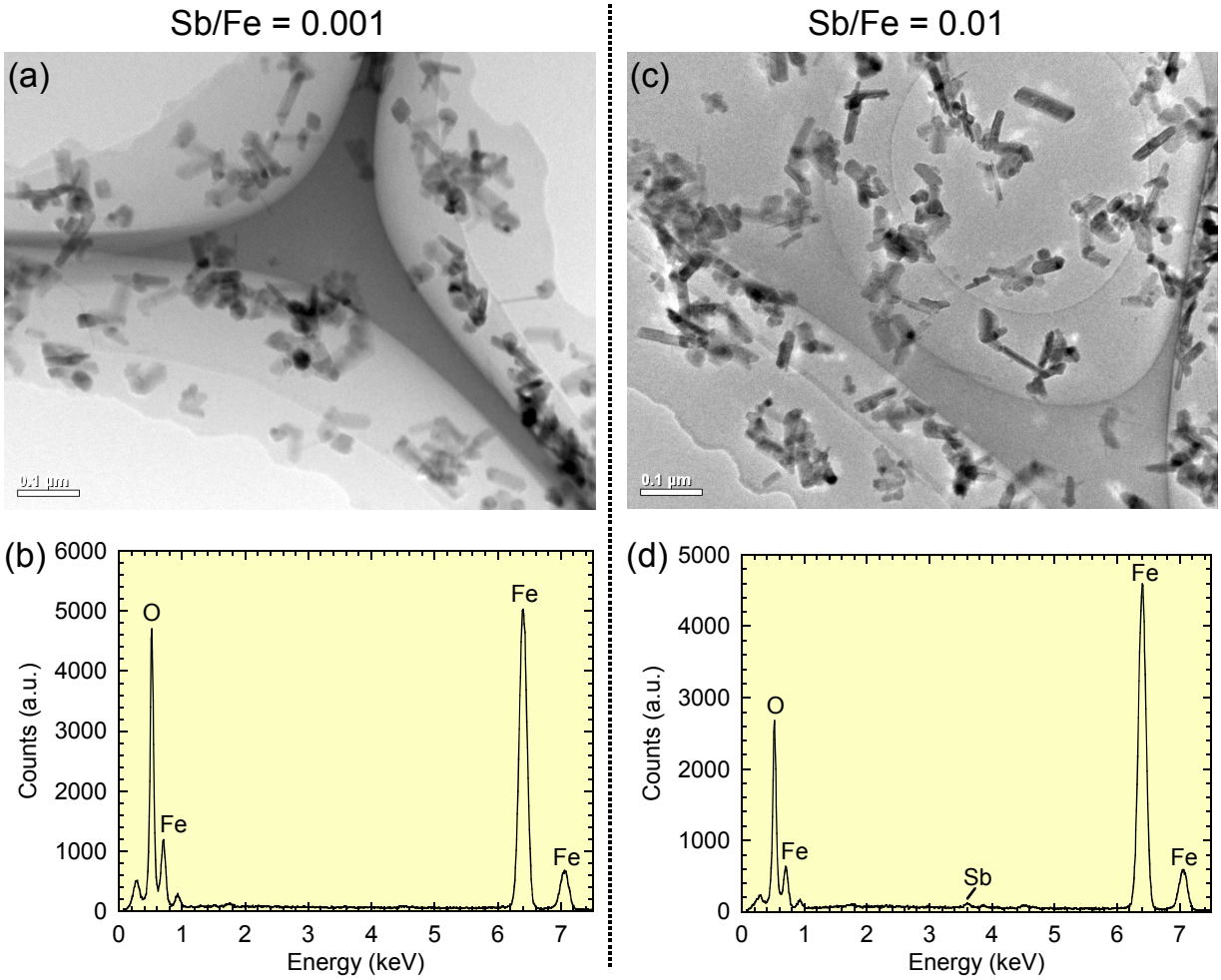

Figure S11. TEM image and single-particle EDS spectrum of 70 days-aged solid samples. (a) and (b): Sb/Fe 0.001 series. (c) and (d): Sb/Fe 0.01 series.

XRD and FT-IR analyses of Sb(V)-coprecipitated goethite and hematite

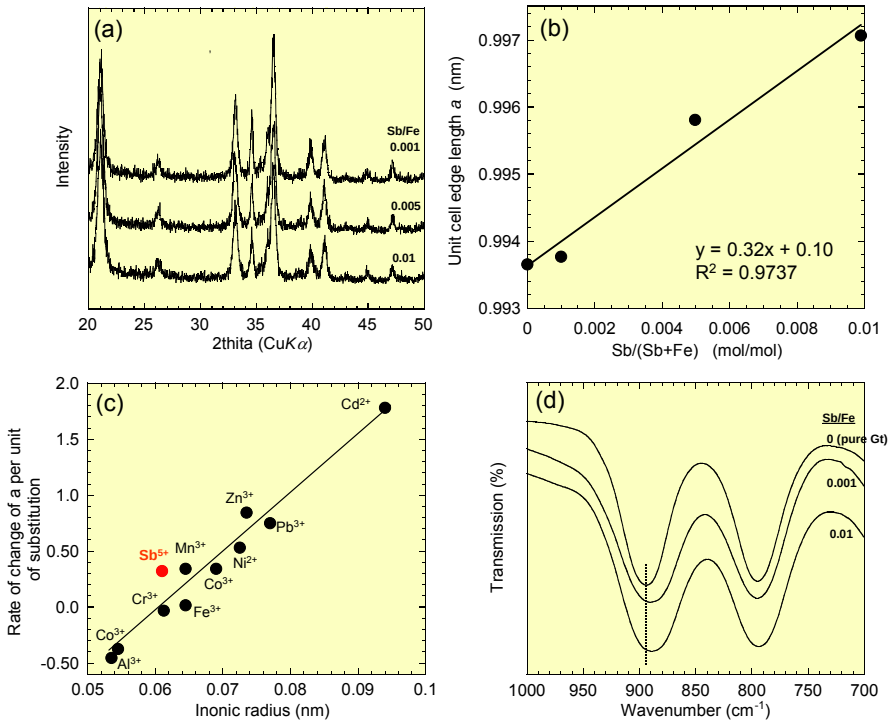

Figure S12. Sb(V)-coprecipitated goethite series. (a) XRD patterns. (b) Relationship between unit cell edge length *a* and substitution amount of Sb(V). (c) Rate of change of *a* per mol of substituted metal (= slope of the upper line) vs. ionic radius of the respective metal cations (Modified from Gerth (1990)). (d) FT-IR spectra in transmission mode.

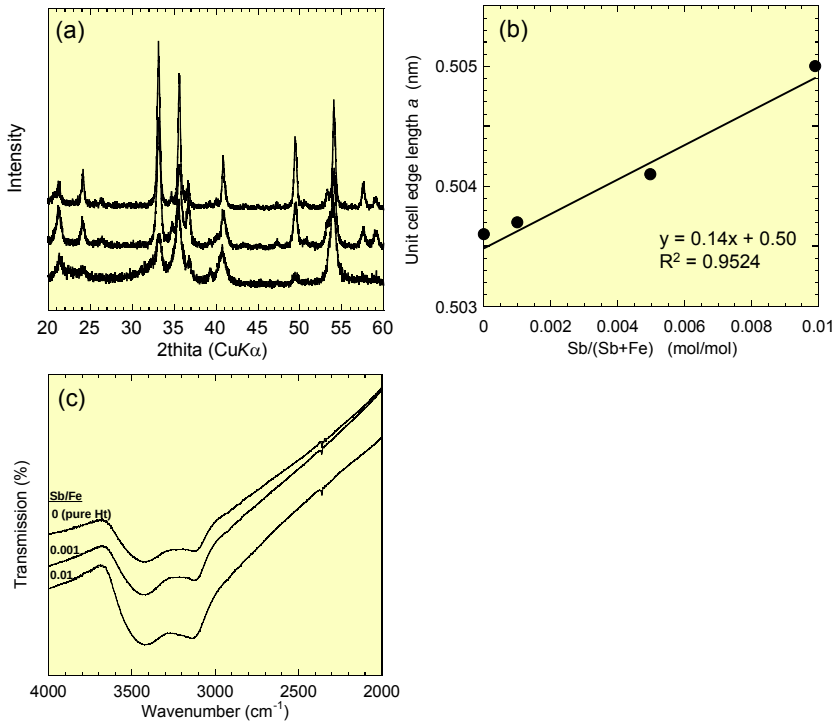

Figure S13. Sb(V)-coprecipitated hematite series. (a) XRD patterns. (b) Relationship between unit cell edge length *a* and substitution amount of Sb(V). (c) FT-IR spectra in transmission mode.

(a) For Fe XAFS measurement

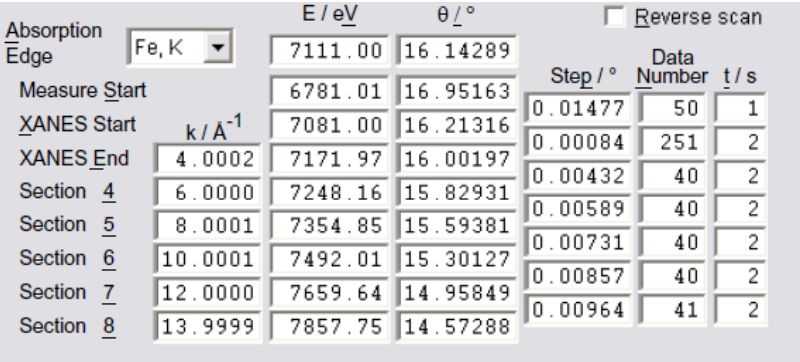

(b) For Sb XAFS measurement

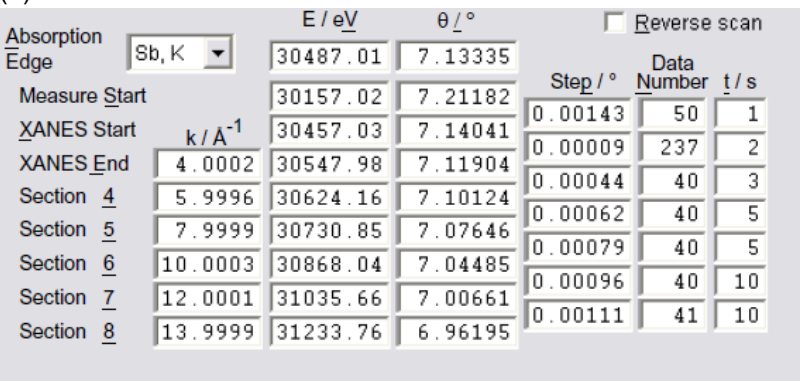

Figure S14. Parameters of EXAFS measurements for Fe (a) and Sb (b)

Table S3. Recovery percentage in phosphate-extraction experiment.

		Sb(V)-adsorbed ferrihydrite Recovery (%)	Sb(V)-adsorbed goethite Recovery (%)	Sb(V)-adsorbed hematite Recovery (%)
Sb/Fe ratio	0.001	95	100	100
	0.005	92	95	98
	0.01	91	94	98

Details of EXAFS analyses.

EXAFS spectra of Fe and Sb were processed using a software package, REX2000 ver. 2.5 (Rigaku Co.). The EXAFS oscillation was extracted from the original spectrum by a spline smoothing method. The threshold energy of Sb and Fe K-edge (E_0) was set at the edge inflection point for all of the samples studied. The edge inflection point was determined from the maximum of the first derivative of XANES spectra. The Fourier transformation of the $k^3\chi(k)$ EXAFS function from k space to r space was performed in the range 2.5-12.0 $Å^{-1}$ for Fe and the range 2.0-13.0 $Å^{-1}$ for Sb to obtain a radial structural function. The inversely Fourier filtered data were analyzed with a least-squares fitting method. The inversely Fourier filtered data were analyzed with a usual curve fitting method. Sb K-edge μ-XAFS measurements were conducted on supply of high energy X-ray beam. To test the effects of possible radiation-induced oxidation and reduction of Sb in soil samples, we collected several successive scans of $KSb^{V}(OH)_6$, $Sb^{III}_2O_3$, and an Sb(V)-coprecipitated ferrihydrite with Sb/Fe ratio of 0.001. Three successive scans of each sample were collected, where it took 20 min for each scan. Both oxidation and reduction induced by radiation were not observed throughout the successive scans of all samples and the quantitative analyses. These results show that there was no photo oxidation or reduction of Sb in the solid samples in 60 min radiation. To avoid the radiation damage, the duration of each scan was limited less than 60 min for an Sb XAFS spectrum on each point in this study and one spectrum was collected at each point.

The fraction of the Fe phases (ferrihydrite, goethite, hematite) in solid samples was determined by a least-squares k^3-weightened EXAFS spectral fitting using Athena interface to IFEFFIT (Newville, 2001).

For quantitative EXAFS simulation for Sb, the intrinsic loss factor (S_0^2) factors were set to 0.85 and 1 for the Sb-O and Sb-Fe shells, respectively. These parameters calibrated from reference compound, tripuhyite. Final fits were obtained for k-space data using REX2000.
The theoretical phase shift and amplitude functions employed in this fitting procedure were extracted from FEFF7.0. Atoms files were written for model compounds (Sb(V)-coprecipitates) and aged samples using a structural model provided by Gualtieri and Venturelli (for goethite), Blake et al. (for hematite), and Michel et al. (for ferrihydrite), using a substituent atom (= Sb) as a core metal (instead of Fe) in the FEFF file. For the Sb(V)-coprecipitated ferrihydrite, we equally assigned Sb(V) atom to the octahedral Fe(III) sites in the unit cell, though the structure model contains three Fe sites including tetrahedral and octahedral sites. For the Sb(V)-coprecipitated goethite and hematite, Sb(V) atom was replaced with the octahedral Fe(III) site. For simulation of Sb-Fe shells of solid samples, we assumed that these predominantly result from backscattering caused by the Fe atom rather than the Sb atom, because the Sb/Fe molar ratio in solids is lower than 1% in the present study. Multiple-scattering (MS) contributions were not considered in Sb EXAFS simulation in the present study, because the contribution with a total path length < 4.0 Å was too small compared with Sb-O and Sb-Fe single path oscillations. We thus ignored the MS contribution in determining of Sb-O and Sb-Fe bond distances by a shell-by-shell fitting.

Literature cited

Blake, R.L.; Hessevick, R.E.; Zoltai, T.; Finger L.W. Refinement of the hematite structure. *Am. Mineral.* **1966**, *53*, 123-129.

Cornell, R.M.; Giovanoli, R. The influence of copper on the transformation of ferrihydrite ($5Fe_2O_3 \cdot 9H_2O$) into crystalline products in alkaline media. *Polyhedron* **1988**, 7, 385-391.

Cornell, R.M.; Giovanoli, R.; Schneider, P.W. Review of the hydrolysis of iron(III) and the crystallization of amorphous iron(III) hydroxide hydrate. *J. Chem. Technol. Biotechnol.* **1989**, 46, 115-134.

Cornell, R.M.; Schwertmann, U. *The Iron Oxides: Structure, Properties, Reactions, Occurrences and Uses.* 2nd and extended ed.; Wiley-VCH: Weinheim, 2003.

Ebinger, M.H., Schulze, D.G. Mn-substituted goethite and Fe-substituted goethite synthesized at acid pH. *Clays Clay Min*. **1989**, *37*, 151-156.

Filella, M.; May, P.M. Computer simulation of the low-molecular-weight inorganic species distribution of antimony(III) and antimony(V) in natural waters. *Geochim. Cosmochim. Acta* **2003**, *67*, 4013-4031.

Fisher, W.R.; Schwertmann, U. The formation of hematite from amorphous iron(III) hydroxides. *Clays Clay Miner*. **1975**, *23*, 33-37.

Fitzpatrick, R.W.; Le Roux, J.; Schwertmann, U. Amorphous and crystalline titanium and iron-titanium oxides in synthetic preparations, at near ambient conditions, and in soil clays. *Clays Clay Miner*. **1978**, *26*, 189-201.

Gasser, R.G.; Jeanroy, E.; Mustin, C.; Barres, O.; Nusch, R.; Berthelin, J.; Herbillon, A.J. Properties of synthetic goethite with Co for Fe substitution. *Clay Min*. **1996**, *31*, 465-476.

Gerth, J. Unit-cell dimensions of pure and trace metal-associated goethites. *Geochim. Cosmochim. Acta* **1990**, *54*, 363-371.

Gualtieri, A.; Venturelli, P. In situ study of the goethite-hematite phase transformation by real time synchrotron powder diffraction. *Am. Mineral.* **1999**, *84*, 895-204.

Hansel, C.M.; Wielinga, B.W.; Fendorf, S. Structural and compositional evolution of Cr/Fe solids after indirect chromate reduction by dissimilatory iron-reducing bacteria. *Geochim. Cosmochim. Acta* **2003**, *67*, 401-412.

Kandori, K., Aoki, Y.; Yasukawa, A.; Ishikawa, T. Effects of metal ions on the morphology and structure of haematite particles produced from hydrolysis reaction. *J. Mat. Chem.* **1998**, *8*, 2287-2292.

Leuz, A.-N.; Monch, H.; Johnson, C.A. Sorption of Sb(III) and Sb(V) to goethite: Influence on Sb(III) oxidation and mobilization. *Environ. Sci. Technol*. **2006**, *40*, 7277-7282.

Manceau, A.; Drits, V.A. Local structure of ferrihydrite and feroxyhite by EXAFS spectroscopy. *Clay Miner.* **1993**, *28,* 165-184.

Michel, F.M.; Antao, S.M.; Lee, P.L.; Chupas, P.J.; Liu, G.; Strongin, D.R.; Schoonen, M.A.A.;

Phillips, B.L.; Praise, J.B. The structure of ferrihydrite, a nanocrystalline material. *Science* **2007**, 316, 1726-1729.

Mitsunobu, S.; Takahashi, Y.; Terada, Y.; Sakata, M. Antimony(V) incorporation into synthetic ferrihydrite, goethite, and natural iron oxyhydroxides. *Environ. Sci. Technol*. **2010**, *44*, 3712-3718.

Nagano, T.; Mitamura, H.; Nakamura, S. Formation of goethite and hematite from neodymium-containing ferrihydrite suspensions. *Clays Clay Min*. **1999**, *47*, 748-754.

Newville, M. IFEFFIT: interactive EXAFS analysis and FEFF fitting. *J. Synchrotron Rad.* **2001**, *8*, 322-324.

Scheinost, A.C.; Rossberg, A.; Venelon, D.; Xifra, I.; Kretzschmar, R.; Leuz, A.-K.; Funke, H.; Johnson, C.A. Quantitative antimony speciation in shooting-range soils by EXAFS spectroscopy. *Geochim. Cosmochim. Acta* **2006**, *70*, 3299-3312.

Schwertmann, U.; Cornell, R. M. *Iron Oxides in the Laboratory,* 2nd ed.; Wiley–VCH: Weinheim, 2000.

Schwertmann, U.; Gasser, U.; Sticher, H. Chromium-for-iron substitution in synthetic goethites. *Geochim. Cosmochim Acta*, **1989**, *53*, 1293-1297.

Shannon, R.D. Revised effective ionic radii and systematic studies of interatomic distances in halides and chalcogenides. *Acta Cryst*. **1976**, *A32*, 751-767.

Singh, B.; Sherman, D.M.; Gilkes, R.J.; Wells, M.; Mosselmans, J.F.W. Structural chemistry of Fe, Mn, and Ni in synthetic hematites as determined by extended X-ray absorption fine structure spectroscopy. *Clays Clay Min*. **2000**, *48,* 521-527.

Stiers, W.; Schwertmann, U. Evidence for manganese substitution in synthetic goethite. *Geochim. Cosmochim Acta* **1985**, *49*, 1909-1911.

Utsunomiya, S.; Kersting, A. B.; Ewing, R. C. Groundwater nanoparticles in the far-field at the Nevada test site: mechanism for radionuclide transport. *Environ. Sci. Technol*., **2009**, *43*, 1293-1298.

Zabinsky, S.I.; Rehr, J.J.; Ankudinov, A.; Albers, R.C.; Eller, M.J. Multiple-scattering calculations of X-ray-absorption spectra. *Phys. Rev. B* **1995**, *52*, 2995-3009.